Available online at www.sciencedirect.com
SCIENCE DIRECT®
European Journal of Mechanics B/Fluids 24 (2005) 167–187

The influence of high free-stream turbulence and a favourable pressure gradient on an incompressible axisymmetric turbulent boundary layer

B. Stefes *, H.-H. Fernholz

Hermann-Föttinger-Institut für Strömungsmechanik, Technische Universität Berlin, Strasse des 17. Juni 135, 10623 Berlin, Germany

Received 18 September 2003; received in revised form 20 April 2004; accepted 3 June 2004

Available online 28 July 2004

Abstract

This experimental study investigates the effect of high free-stream turbulence intensity $Tu_\delta \leqslant 13\%$ on a turbulent boundary layer in a strong favourable pressure gradient $K = (\nu/u_\delta^2)(\mathrm{d}u_\delta/\mathrm{d}x) \leqslant 3.6 \times 10^{-6}$. The Reynolds number Re_{δ_2} at the beginning of the favourable pressure gradient (FPG) is about 1200. The pressure gradient and the free-stream turbulence (FST) affect the development of the boundary layer, but the decay rate of Tu_δ in the streamwise direction depends both on the magnitude of the initial level of Tu_δ and on the pressure distribution. Therefore, two boundary layers were investigated in detail with the same pressure distribution but with different initial levels of FST. The investigation showed that only a high FST level reduced the relaminarization of the boundary layer which occurred without FST and less so at small FST. Extensive hot-wire and skin-friction measurements were made and the data comprise mean velocity profiles, Reynolds stresses, velocity correlations, integral length scales and power spectra for the streamwise velocity component.

Keywords: Turbulent boundary layer; High free-stream turbulence; Favourable pressure gradient

1. Introduction

Strong favourable pressure gradients, high levels of free-stream turbulence and Reynolds-number effects dominate the behaviour of boundary layers in gas turbine engines. The state of the boundary layer can be laminar, transitional, turbulent or relaminarescent and the pressure distribution affects the decay of the FST level in streamwise direction. This renders the determination of heat transfer and skin friction a rather difficult problem and its solution has high priority for many practical applications. In order to facilitate a solution of this complex problem investigations always dealt only with the influence of selected parameters of the problem.

Since the heat transfer rate is greatly different in laminar and turbulent boundary layers much attention has been focused on how FST affects transition both in zero pressure gradient (ZPG) and favourable pressure gradient (FPG) boundary layers (e.g. Abu-Ghannam and Shaw [1], Roach and Brierly [2], Mayle [3], Blair [4,5], Mayle et al. [6]). The effect of FST on two-dimensional incompressible turbulent boundary layers with zero pressure gradient has been investigated, for example, by

* Corresponding author.
E-mail address: Bruno.Stefes@airbus.com (B. Stefes).

0997-7546/$ – see front matter
doi:10.1016/j.euromechflu.2004.06.004

Table 1
Parameters of the four cases at the first measuring station $x = 0.828$ m and the maximum acceleration parameter K at station $x = 1.453$ m

Case	r_{jet}	Tu_δ [%]	$\delta_{99.5}$ [mm]	δ_2 [mm]	Re_{δ_2}	H_{12}	$c_f \times 10^3$	$K_{\max} \times 10^6$
1	0	0.8	17.7	1.85	993	1.47	4.21	3.54
2	2.5	5.0	47.0	3.85	2019	1.35	3.97	3.35
3	4.4	10	68.5	3.64	1822	1.27	4.64	3.51
4	6.3	13	68.5	3.31	1732	1.25	4.89	3.64

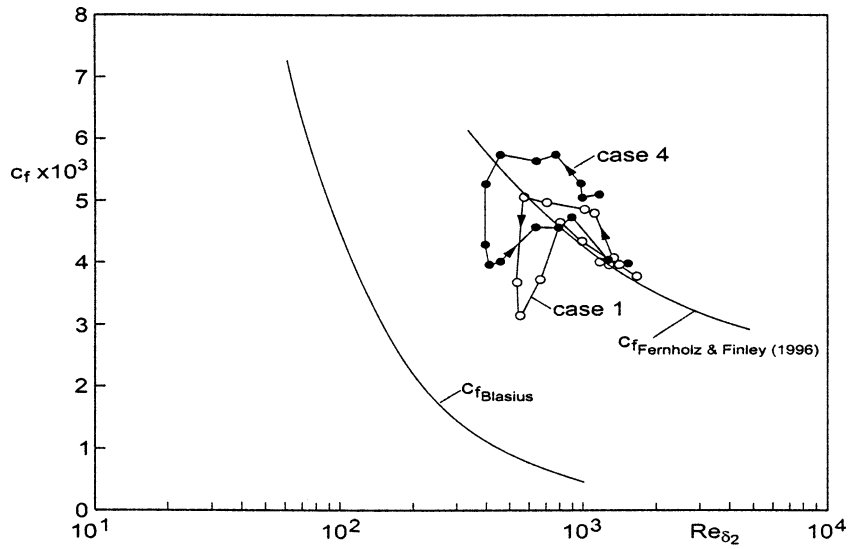

Fig. 1. The (c_f, Re_{δ_2})-plane for FPG boundary layers with laminarescent behaviour (Cases 1 and 4).

Blair [7,8], Castro [9] and Hancock and Bradshaw [10,11] using bar-grid generated FST with intensities $Tu_\delta \leqslant 8\%$. In gas turbines, FST levels of up 20% are possible (Mayle [3]) and therefore new ways had to be found for laboratory experiments to generate much higher levels of FST than can be obtained from bar-grids (for a survey see Thole et al. [12]). Thole and Bogard [13,14] developed a turbulence generator which uses air jets injected normal to the mainstream flow, a technique which achieves FST levels of up to 20% and investigated a turbulent boundary layer with ZPG. There are far fewer experiments dealing with the joint effect of FST and a favourable pressure gradient on a boundary layer fully turbulent on the test wall. The two test cases investigated by Blair [4] showed no transition effects without FST. Rued and Wittig [15] considered boundary layers subject to favourable pressure gradients and cooling of the wall with the acceleration parameter K as high as 5.7×10^{-6} and $Tu_\delta \leqslant 11\%$. Re_{δ_2} at the start of the FPG is not given but estimated to be in the low Reynolds number range. In a more recent study Volino and Simon [16] investigated boundary layer transition on a concave wall under strong acceleration conditions $K \leqslant 9.7 \times 10^{-6}$, for $Tu_\delta \leqslant 8\%$ and $Re_{\delta_2} = 275$ at the inlet to the test section (no truly turbulent boundary layer).

Warnack and Fernholz [17] – henceforth denoted WF – carried out measurements in highly accelerated fully turbulent boundary layers with very low FST $Tu_\delta \leqslant 0.1\%$ and found relaminarization of the boundary layer. This is the third class of three archetypes of reverting flows suggested by Narasimha [18] where a turbulent boundary layer is subjected to severe acceleration. Reversion to laminar-like flow occurs predominantly by the domination of pressure forces over slowly responding Reynolds stresses in the outer region. This scenario has now been extended by adding FST as an additional parameter. The present experimental study uses approximately the same flow conditions as WF [17] and investigates the combined effect of strong favourable pressure gradient $K \leqslant 3.6 \times 10^{-6}$ and four upstream FST levels $Tu_\delta \leqslant 13\%$ on the streamwise development of an axisymmetric boundary layer and its tendency towards relaminarization. In order to separate the effects of acceleration and FST a series of tests at the same FST levels were conducted in a zero-pressure gradient boundary layer in the same test section (Stefes and Fernholz [19]).

Two of the four cases measured in the accelerated flow (Case 1 with low FST and Case 4 with high FST) are discussed in more detail in this paper (for Cases 2 and 3 see Stefes [20]). Some parameters of the four cases at the first measuring station are given in Table 1.

The development of the skin-friction parameter $c_f = 2\bar{\tau}_w/(\rho_\delta u_\delta^2)$ and the Reynolds number $Re_{\delta_2} = \delta_2 u_\delta/\nu$ (Fig. 1) compared with their relationships in laminar and turbulent boundary layers with ZPG and low FST presents a useful first overview

(see also WF [17] and Volino and Simon [16]). Due to the acceleration and the FST the skin friction is higher than in a ZPG boundary layer in both cases. The decrease of c_f is considerably stronger in Case 1 than in Case 4 where the high FST keeps the mean velocity profiles fuller and c_f higher. So the boundary layer is kept further away from relaminarization than in Case 1. Both boundary layers relax to c_f-values of a ZPG flow in the downstream region of the test section.

Besides the mean flow quantities, this investigation presents the development of the Reynolds normal and shear stresses, of some higher moments of the fluctuating velocities and the wall shear stress, of the integral length scales, of the turbulence production and of the spectra.

2. Experimental facility

The experiments were performed in the low-turbulence wind tunnel of the Hermann-Föttinger-Institut. The wind tunnel is a closed return facility with a centrifugal fan and a 25 kW motor and an additional 1 kW blower to remove the nozzle boundary layer at the start of the test section (for details see Fernholz and Warnack [21]). The axisymmetric test section (6 m length) consisted of Perspex pipe sections (0.44 m inner diameter) of various lengths, one of which had an elliptical leading edge (6 : 1) and determined the origin of the test boundary layer on the wall of the test section. The air temperature was kept constant within $\pm 0.1\,^{\circ}\mathrm{C}$. The flow velocity at the entry of the test section was below 10 m/s and could be controlled to 0.3%.

The favourable pressure distribution for the four cases investigated was generated by an axisymmetric displacement body situated along the centreline of the test section (Fig. 2) with the stagnation point 1.218 m downstream of the leading edge (cf. WF [17], Case 2). The displacement body was held by radial rods (6 mm in diameter) attached at the rear part so that the boundary layer under investigation was not disturbed (for further detail see WF [17]).

The turbulence generator was situated between the nozzle exit and the test section and consisted of a cylindrical pipe section, the wall of which had holes to inject the air jets normal to the mainstream. The air supply for the jets was provided by a blower via a circular settling chamber (Fig. 2) and was uniform within ±1.5%. The diameter D of the jet holes was 20 mm and their centres were $3D$ apart around the circumference, as suggested by Thole and Bogard [14]. A perforated metal cylinder along the centreline of the turbulence generator and an adjacent perforated metal cone served to smooth the interaction of the jet and the mean velocity distribution. For the generation of the FST the ratio of the jet and mainstream velocities r_{jet} was varied between 0 and 6.3, generating at the first measuring station the FST levels given in Table 1. For Case 1 the FST was generated by the perforated metal cylinder and cone without air injection. The downstream end of the turbulence generator was 0.265 m upstream of the leading edge of the test-section wall ($x = 0$) (for further details see Stefes [20]).

The turbulence generator was optimized to achieve a largely uniform mean velocity distribution in a region between 50 and 100 mm normal to the wall which determined the free-stream turbulence level for the boundary layer. In the centre region of the test section the mean velocity distributions show a wake-like behaviour and the fluctuating velocities a plateau for Cases 1 and 2 and almost uniform distributions for Cases 3 and 4 (for details see Stefes and Fernholz [19], Stefes [20]). Both, wakes

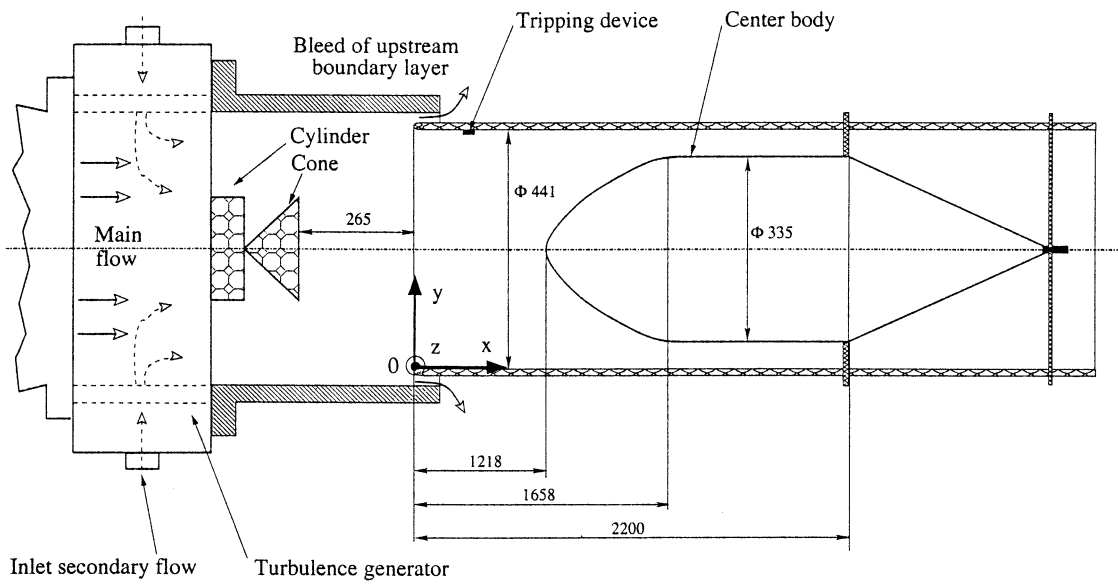

Fig. 2. Test section with turbulence generator and centre body (not to scale).

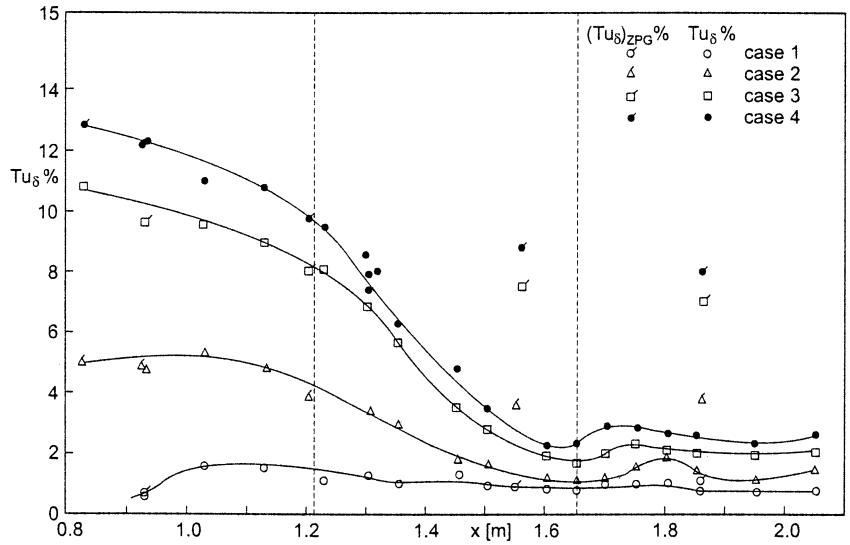

Fig. 3. Distribution of the free-stream turbulence level Tu_δ in streamwise direction in zero- and favourable-pressure gradients (lines are for visual aid only). The vertical lines mark the beginning and the end of the convergence of the center body.

and plateaus, level off in downstream direction. The free-stream is defined here as the region in which the intensities cease to vary with y.

The distribution of the FST intensity Tu_δ in streamwise direction defined as $(\overline{u'^2_\delta})^{1/2}/u_\delta$ is shown in Fig. 3. The favourable pressure gradient enhances strongly the decrease of Tu_δ and, the decay rate grows with increasing initial turbulence level. For comparison some data are also plotted which were obtained in the same test section with the centre-body removed. They show that the decay rate of Tu_δ is much smaller in a ZPG mainly because the free-stream velocity remains constant. The anisotropy parameter $(\overline{v'^2}/\overline{u'^2})^{1/2}$ in the range of the ZPG upstream of the acceleration region settles down to values between 0.85 (Case 4) and 1 (Case 1) in the freestream.

Earlier investigations in ZPG boundary layers have shown that the effect of FST depends significantly on both the free-stream intensity and a length scale ratio, for example the u'-component streamwise integral length scale Λ_{11} and the boundary-layer thickness $\delta_{99.5}$. The effects of FST on the boundary layer were found to be strong, if the ratio $\Lambda_{11}/\delta_{99.5}$ is about one (Hancock and Bradshaw [10]). This behaviour holds in turbulent boundary layers with ZPG where the boundary layer thickness grows only slowly. In an accelerated boundary $\delta_{99.5}$ can vary significantly and therefore the development of $\Lambda_{11}/\delta_{99.5}$ needs special attention.

The behaviour of the large structures in the free-stream and in the boundary layer affected by acceleration was investigated by measuring the autocorrelation R_τ to obtain the length in streamwise direction x and the space correlation $R^{\Delta y}_{u'u'}$ in the direction y normal to the wall. From these the integral length scales

$$\Lambda_{11} = \Lambda_\tau \bar{u} \tag{1}$$

with

$$\Lambda_\tau = \int_0^\tau R_\tau \, \mathrm{d}\tau \tag{2}$$

and

$$\Lambda_{12} = \int_0^{\Delta y} R^{\Delta y}_{u'u'} \, \mathrm{d}y \tag{3}$$

were calculated. In (1) Taylor's hypothesis was assumed to hold.

Since the interactive effect of FST and pressure gradient is very different in Cases 1 and 4 the distributions of the integral length scales Λ_{11} and Λ_{12} at the edge of the boundary layer in streamwise direction are first shown in dimensional form (Fig. 4). In the upstream ZPG region Λ_{11} is larger by a factor of 6 in Case 4 compared with Case 1 and rises by about 40% to a peak

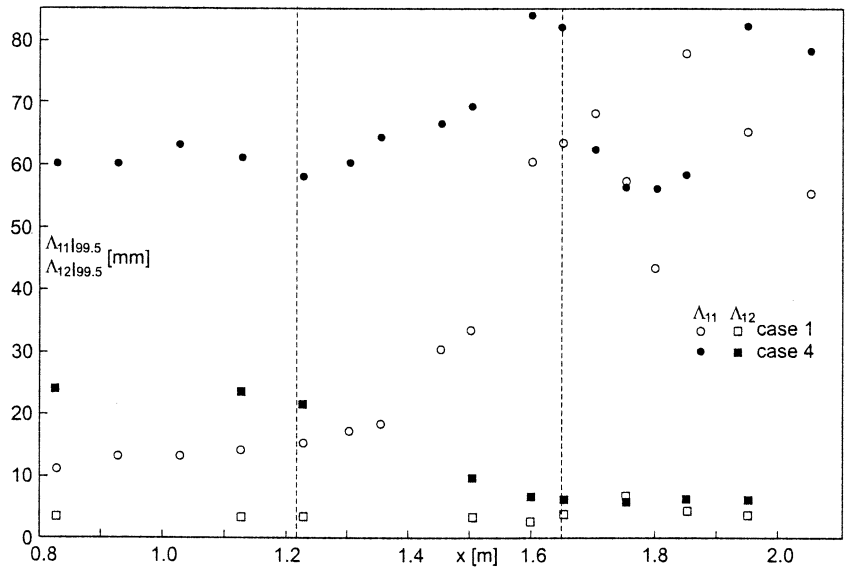

Fig. 4. Distribution of the integral length scales Λ_{11} and Λ_{12} at the edge of the boundary layer in streamwise direction for Case 1 (LFST) and Case 4 (HFST).

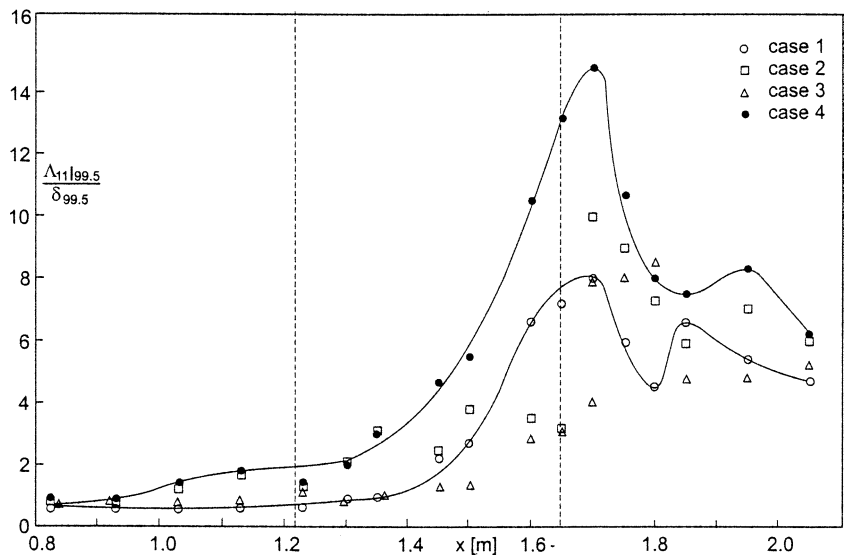

Fig. 5. Distribution of the ratio $\Lambda_{11|\delta_{99.5}}/\delta_{99.5}$ of the integral length scale and the boundary layer thickness in streamwise direction in zero- and favourable-pressure gradients (lines are for visual aid only).

at the end of the acceleration region. In Case 1 Λ_{11} begins with a much smaller length but increases through the acceleration region by about a factor of 6. This elongation could be explained by a shift of the u'-contribution towards the low-wavenumber end of the spectrum which is stronger in the low FST case than in Case 4 where the energy content of the spectrum is higher a priori at the low wavenumbers (see also Launder [22] and WF [17]). In both cases the length of the structures in the x-direction decreases in the ZPG region downstream but rises again before it finally falls in the ZPG boundary layer. For this latter peak we have as yet no explanation. The wall normal integral length scale Λ_{12} in Case 4 exceeds its respective value of Case 1 again by a factor of 6 and then falls through the acceleration region to almost the same value as is reached in Case 1 in the relaxation region with ZPG. The ratio of $\Lambda_{11}/\Lambda_{12}$ (not shown) varies between approximately 3 at the beginning ($x = 0.828$ m) and 7 and 15, respectively, in the acceleration region for Cases 1 and 4.

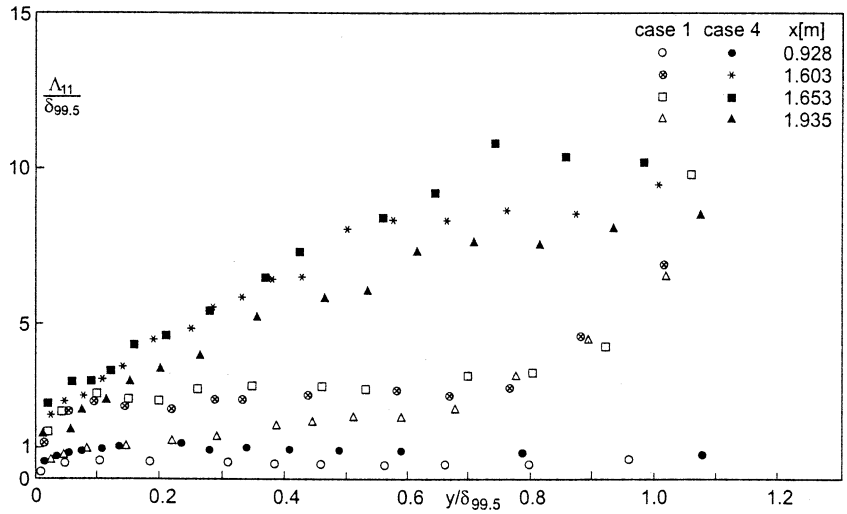

Fig. 6. Profiles of $\Lambda_{11}/\delta_{99.5}$ in outer-law scaling in a favourable pressure gradient with high (Case 4) and low (Case 1) free-stream turbulence at 4 characteristic stations in streamwise direction.

Fig. 5 presents the distribution of $\Lambda_{11|_{\delta_{99.5}}}/\delta_{99.5}$ for the four cases complementing Fig. 4. In all cases the dimensionless length scale is about one in the upstream region – as required to achieve the greatest effect of the FST on the boundary layer – before it rises to its respective peaks. In Case 4 it should be borne in mind that $\delta_{99.5}$ decreases by a factor 15 whereas in Case 1 the factor is 2.5 only. Nevertheless the increase is caused by a large Λ_{11} and a small $\delta_{99.5}$. In the downstream relaxation region $\Lambda_{11}/\delta_{99.5}$ reaches a value of 5.5 which is still far from its initial value. There is good qualitative agreement between the present measurements and those of WF [17] for Case 1 with low FST (note, however, the different definitions for Λ_{12}).

Fig. 6 shows the profiles of $\Lambda_{11}/\delta_{99.5}$ normal to the wall at four characteristics x-stations for Cases 1 and 4. The pattern observed for the length scales in the free-stream is repeated in the boundary layer. The coherent structures at high FST exceed in length those at low FST by about a factor of 3 in and downstream of the acceleration region. Again, the profiles furthest downstream are still far from their initial profiles in both cases.

3. Measuring techniques

Static pressure was measured by a single static tap (0.70 mm diameter) inserted in an interchangeable plug which could be moved in the streamwise direction, using a slot in the test wall (for details see Fernholz and Warnack [21]). MKS Baratron 220 CD pressure transducers were used in the ranges 0–100 and 0–1000 Pa and a HP digital voltmeter 34 970 A with an integrating multiplexer. For the pressure measurements 60 samples (at a frequency of 1 Hz) were taken for the average value and 120 for the Preston-tube calibrations.

Errors in pressure measurements are less than $\pm 0.4\%$, giving the pressure gradient in the highly accelerated region to an accuracy of about 2.5%.

Skin friction was measured by a wall hot-wire probe which proved to be a simple and reliable measuring device for boundary layers with high FST, strong favourable pressure gradients and relaminarescent regions enclosed in turbulent flow (for a comparison with other techniques the reader is referred to Fernholz and Warnack [21], and to Stefes and Fernholz [19]). The wall hot wire was 0.030 mm away from the wall ($y^+ \approx 2$) and the probe was calibrated by means of a Preston tube with the Patel [23] calibration curve. The wall hot wires had a ratio of active wire length l to diameter d of 200 and $l^+ = lu_\tau/\nu$ never exceeded a value of 35. The skin-friction data should be correct within a range of $\pm 4\%$.

Mean and fluctuating components of the velocity were measured using miniature single and X-wire probes with the stem (3 mm diameter) protruding through plugs in the test wall. The prongs of the crossed-wire probe were mounted at the corners of a square of side length 1.5 mm and the tungsten/platinum wires, gold plated at the ends, had an active length of 0.55 mm and a diameter of 2.5 μm (these latter data hold also for the wall hot wire).

The constant-temperature hot-wire anemometer was an IFA 100 from TSI and data acquisition was achieved using a PC with a 16 bit A/D converter on a data acquisition board. The probes were traversed in general away from the wall using an electrically driven traverse gear with an incremental resolution of 0.001 mm. 524k samples (at a frequency of 20 kHz) were taken for all velocity measurements. For the wall hot wire the sampling frequency was 20 kHz (1048k samples).

The uncertainties in the measurements of the fluctuating streamwise and normal velocity components u' and v' are 2% and 5%, respectively and amount to about 10% for $\overline{u'v'}$.

4. Discussion of the mean-flow data

In the following discussion of the boundary layer data attention is focused on Cases 1 (low FST) and 4 (high FST). The other two cases are documented in Stefes [20].

By analogy with WF [17], a survey of the flow is given first by presenting the development of the acceleration parameter $K = (\nu/u_\delta^2)(\mathrm{d}u_\delta/\mathrm{d}x)$, the Reynolds number $Re_{\delta_2} = \delta_2 u_\delta/\nu$, where δ_2 is the momentum loss thickness and u_δ the mean velocity at the edge of the boundary layer, the skin-friction coefficient $c_f = 2\bar{\tau}_w/(\rho_\delta u_\delta^2)$ and the shape parameter $H_{12} = \delta_1/\delta_2$. The mean wall shear stress $\bar{\tau}_w$ was measured by the wall mounted hot-wire probe and δ_1 (displacement thickness) and δ_2 are defined for an axisymmetric internal flow (see Fernholz and Warnack [21]).

Figs. 7(a) (Case 1) and 7(b) (Case 4) show that the pressure distributions, represented by the acceleration parameter K, are in good agreement with each other (the same centre body). Small discrepancies are due to the uncertainty associated with differentiating the measured pressure distributions which are given by Stefes [20]. With an equivalent pressure distribution, the differences in the parameter distributions must be caused by the different decay rates of the FST and its initial turbulence levels,

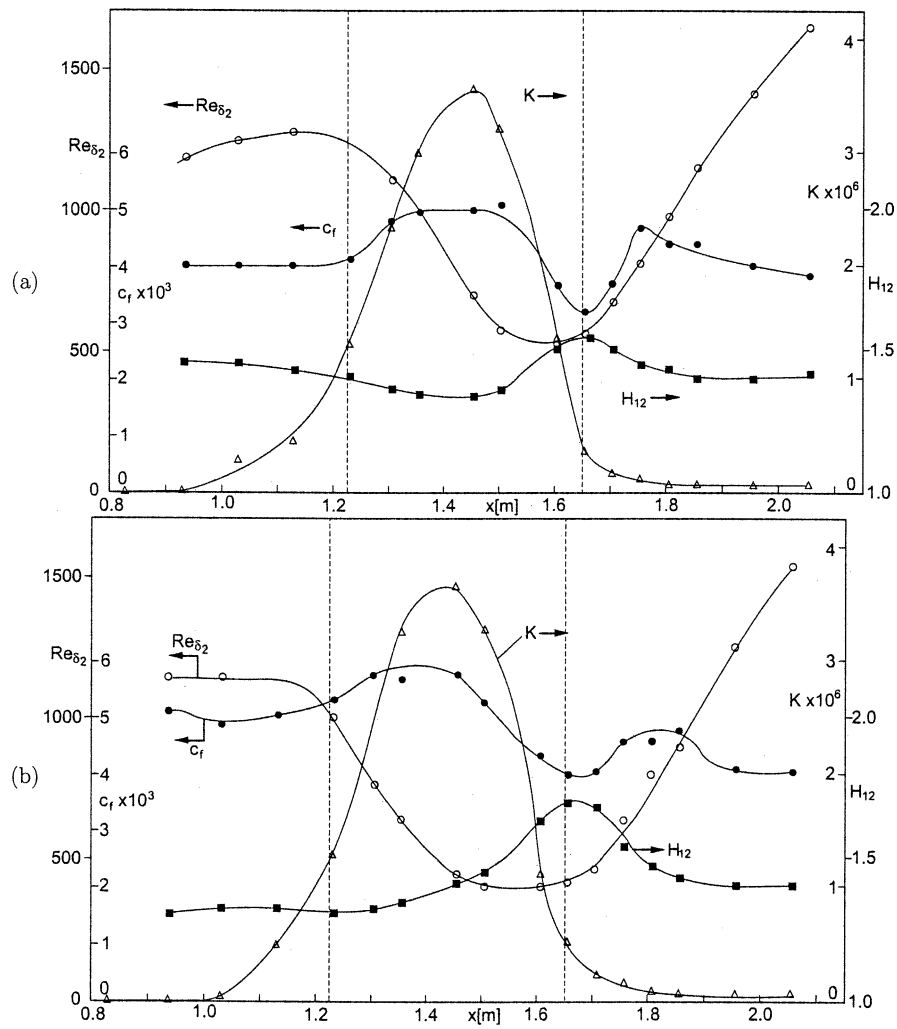

Fig. 7. Streamwise development of the Reynolds number Re_{δ_2}, the shape parameter H_{12}, the skin-friction coefficient c_f and the acceleration parameter K in a FPG boundary layer with FST (lines are for visual aid only). (a) Case 1, low FST. (b) Case 4, high FST.

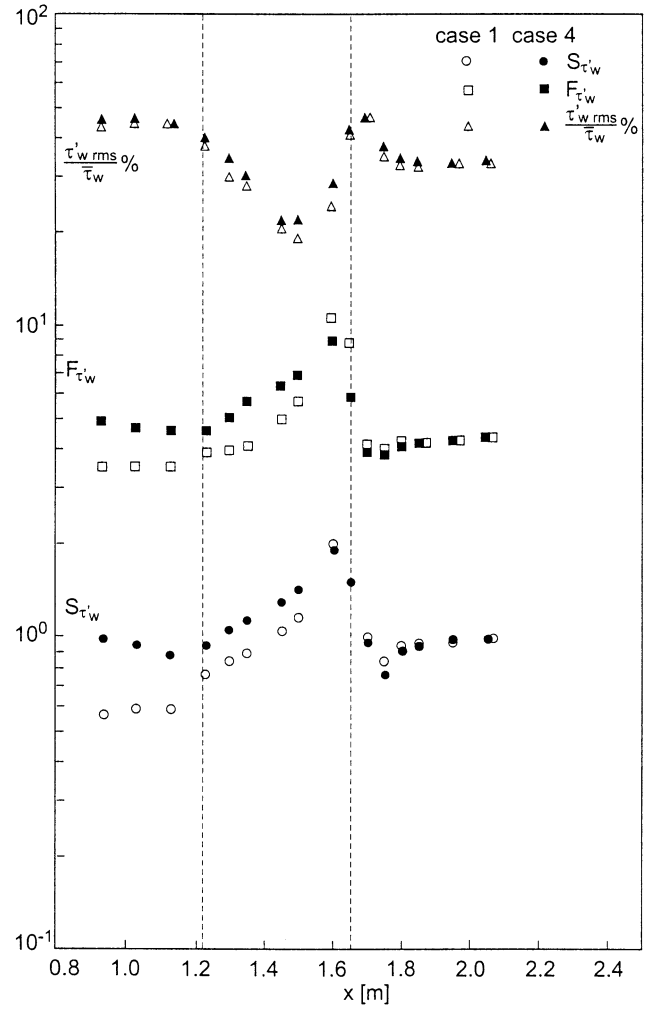

Fig. 8. Streamwise development of the skin-friction fluctuation, the skewness $S_{\tau'_w}$ and flatness $F_{\tau'_w}$ (at about $y^+ \approx 2$) in a FPG turbulent boundary layer with low (Case 1) and high (Case 4) FST.

leading for Case 4 to a fuller initial mean velocity profile. This is characterized by a lower value of $H_{12} = 1.30$ and a higher value of c_f (5.1×10^{-3}) than for Case 1. In Case 4 the level of the c_f-distribution remains higher through the acceleration region causing the boundary layer to stay further away from relaminarization (see also Fig. 1). Re_{δ_2} reacts first to the acceleration, falling from a maximum of about 1200 to a minimum of 400 and 530, respectively, for Cases 4 and 1 and then rising to about 1550 in the downstream ZPG boundary layer. Following the pattern of a fully turbulent accelerated boundary layer in the entry region (see WF [17]), the skin-friction coefficient rises to its first peak close to which K has its maximum value. Downstream of this peak both Re_{δ_2} and c_f fall to their respective minimum values which coincide with the maximum values of H_{12} at the end of the acceleration region. In this region the mean velocity profiles show their largest departure from the logarithmic law (see Figs. 9(a) and 9(b)). At the end of the acceleration region the turbulence production (see Fig. 12) is reactivated and c_f and Re_{δ_2} rise again. Both c_f and H_{12} adapt to values which are only a function of Re_{δ_2} in a zero-pressure-gradient boundary layer, although with a slightly elevated level of free-stream turbulence (see also Case 2 of WF [17] where the level of the FST is negligible).

In this context it is appropriate to compare the "foot prints" of the two boundary layers on the wall by discussing the streamwise development of the skin-friction fluctuation $(\overline{\tau_w'^2})^{1/2}/\overline{\tau_w}$ and the skewness $S_{\tau'_w}$ and flatness $F_{\tau'_w}$ (Fig. 8). The fluctuating quantities in the immediate vicinity of the wall ($y^+ \approx 2$), are dominated by the pressure distribution and less so by the free-stream turbulence level. The latter has no noticeable influence on c'_f but both skewness and flatness are increased by the FST in the upstream region in agreement with the mean skin friction. $S_{\tau'_w}$ and $F_{\tau'_w}$ show peaks in both flow cases at

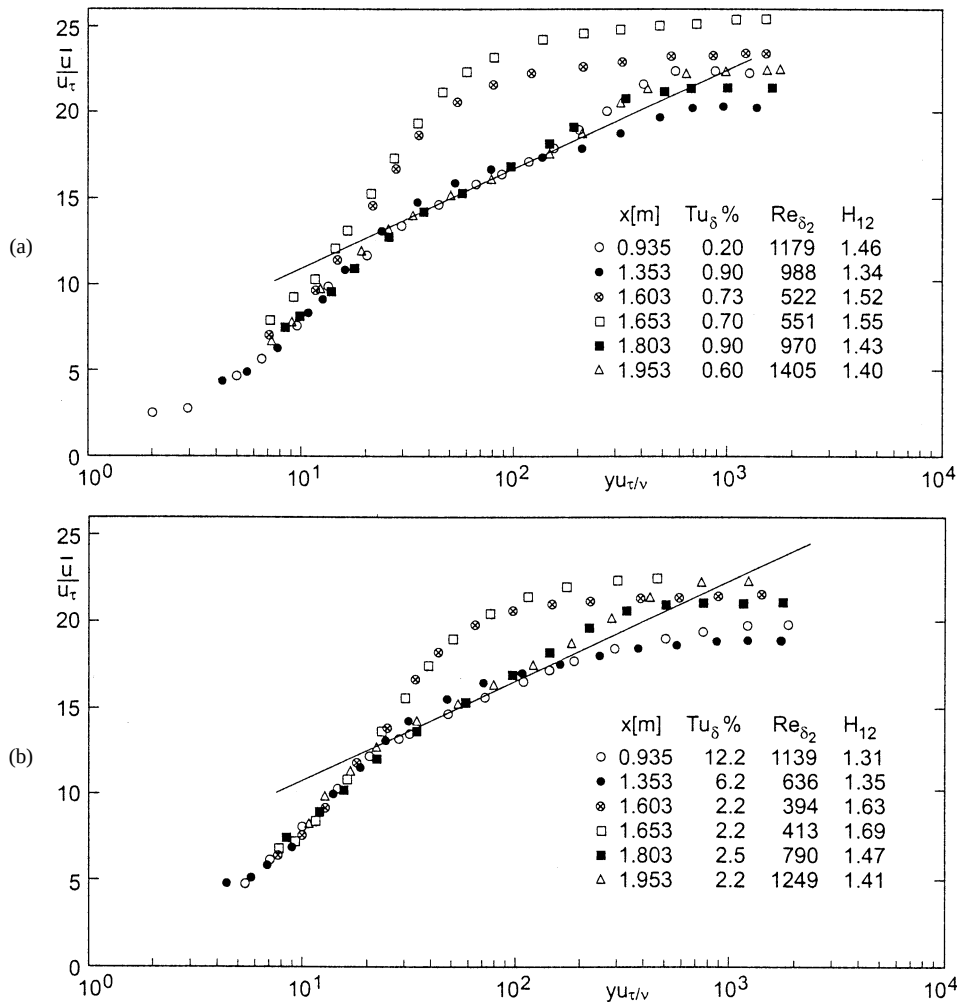

Fig. 9. Profiles of the mean velocity in inner-law scaling in a turbulent boundary layer with a favourable pressure gradient. (a) Case 1, low FST. (b) Case 4, high FST.

about $x = 1.603$ m where Re_{δ_2} reaches it minimum and slightly upstream from the maximum value of H_{12}. Compared with their initial values, $S_{\tau_w'}$ and $F_{\tau_w'}$ rise approximately by a factor 3 and 2 for Cases 1 and 4. The rise of $F_{\tau_w'}$ is indicative of the occurrence of large velocity spikes in the vicinity of the wall. Since these spikes are indicators of the reappearance of high-frequency turbulent bursts superimposed on the relatively low-frequency residual turbulence (Launder [22]), they are relatively smaller in Case 4 which is further away from relaminarization (see also WF [17] and Warnack [24]). The latter author discussed the development of $S_{\tau_w'}$ and $F_{\tau_w'}$ in great detail (his Case 2, which is comparable with the present Case 1) using time series of the skin friction at various stations in streamwise direction.

Figs. 9(a) and 9(b) present the mean-velocity profiles in inner-law scaling in comparison with the standard logarithmic law of the wall (the constants are $k = 0.40$ and $C = 5.10$). The legend of the figures gives the corresponding values of x, Tu_δ, Re_{δ_2} and H_{12} to facilitate a comparison with Figs. 3 and 7(a) and 7(b). At $x = 0.935$ m, where the pressure gradient is still zero, the profiles of Cases 1 and 4 share a certain length of the logarithmic region but show differences in the wake region due to the different levels of the FST. At the following stations FST and pressure gradient effects interact with one another, much more, however, in Case 4 where the FST level is higher. The FST diminishes the favourable pressure gradient effect in that it reduces the departure from the standard log-law and thus opposes the development towards a laminar-like profile as was observed by WF [17] (their Figs. 5 and 6) for very low FST. The maximum values of $\bar{u}/u_\tau$ were 28 (WF [17]), 25 (Case 1) and 22 (Case 4) in order of increasing FST levels. As already noticed by WF [17], the profile with the largest departure from the standard log law is that for which H_{12} has its maximum and c_f its minimum. At this position ($x = 1.653$ m) one also finds a maximum of the fluctuating skin friction and its higher moments (Fig. 8).

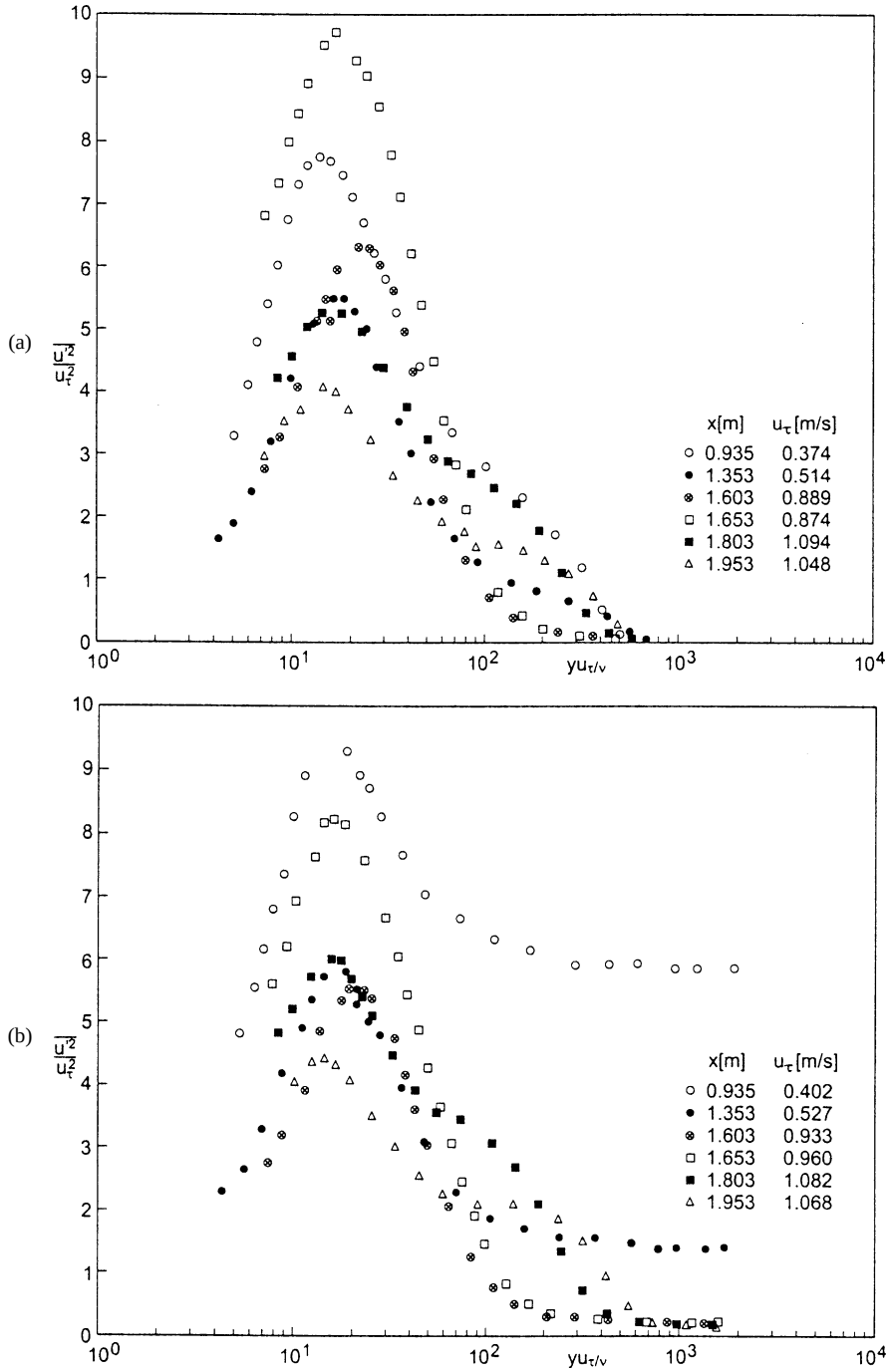

Fig. 10. Profiles of Reynolds normal stress component $\bar{\rho}\overline{u'^2}$ in inner-law scaling in a turbulent boundary layer with a FPG and FST. (a) Case 1, low FST (symbols as in Fig. 9(a)). (b) Case 4, high FST (symbols as in Fig. 9(b)).

5. Discussion of the turbulence data

Only two of the Reynolds normal stresses and the Reynolds shear stress $-\bar{\rho}\overline{u'v'}$ were measured due to time limitations. Figs. 10(a) and 10(b) show the profiles of the component in streamwise direction $\bar{\rho}\overline{u'^2}$, in inner-law scaling for Cases 1 and 4. The peak value of $\overline{u'^2}/u_\tau^2$ (Case 1) increases by about 30% between the location of the initial profile and $x = 1.653$ m where

H_{12} reaches its peak. Further downstream, the level of the profiles decreases sharply until $(\overline{u'^2}/u_\tau^2)_{\max}$ at the last measuring station is only half its value in the initial profile. This is partly due to the much higher skin-friction velocity and partly to the turbulence structure which has not yet reached equilibrium, i.e. higher values of u'. The profiles of Case 1 are in good qualitative agreement with the earlier measurements of WF [17] (see their Fig. 12).

For Case 4 with high FST (Fig. 10(b)) the absolute maximum of $\overline{u'^2}/u_\tau^2$ is reached at the location of the initial profile where the FST has its maximum value, followed by the value at the location where H_{12} reaches its peak value ($x = 1.653$ m). Compared with the normal stress profiles in Fig. 10(a) the two upstream profiles have a higher level of $\overline{u'^2}$ because of the high FST. With the FPG increasing and the FST level falling in streamwise direction the influence of the favourable pressure gradient becomes dominant and the development of the profiles becomes similar to Case 1. In both cases the location of the peaks moves out from $y^+ \approx 14$ to about 22 where the acceleration is strongest and then moves in again with the relaxation

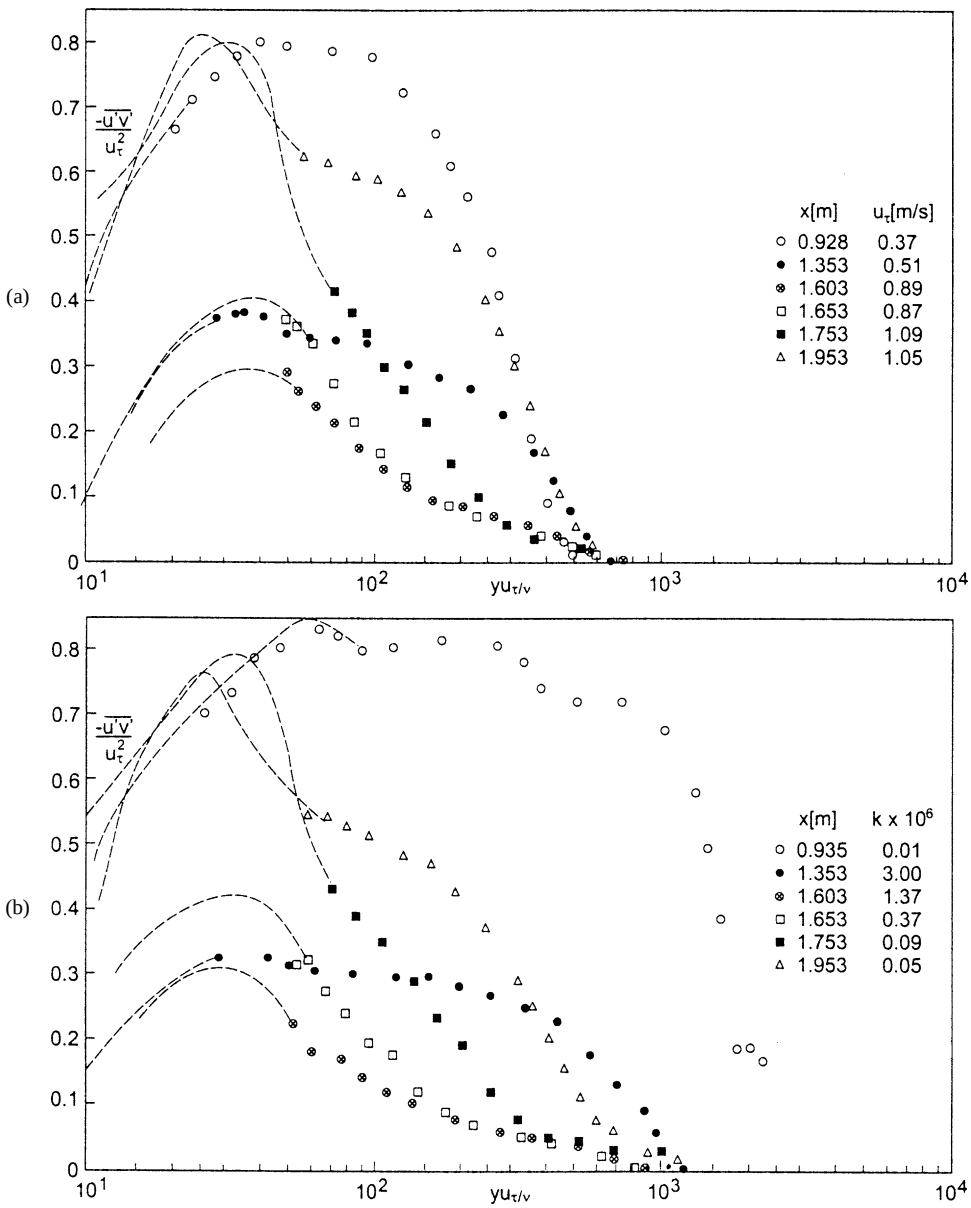

Fig. 11. Profiles of Reynolds shear stress component $\bar{\rho}\overline{u'v'}$ in inner-law scaling in a turbulent boundary layer with a FPG and FST. (a) Case 1, low FST (symbols as in Fig. 9(a)). (b) Case 4, high FST (symbols as in Fig. 9(b)). Symbols denote measured data, the dashed lines calculated data.

of the pressure gradient. The overall level of the Reynolds normal stress is much reduced by the FPG and this is reflected in the profiles of the production term (see Fig. 12). The profiles of the Reynolds normal stress do not approach yet those of an undisturbed ZPG boundary layer at the last measuring station (see Fernholz and Finley [25], their Fig. 15) indicating that the recovery process will need a much longer distance when FST and FPG have influenced the boundary layer upstream. This recovery process begins first in the outer layer ($x = 1.953$ m) while the inner peak is still falling. For a full recovery it should rise again to a maximum value of about 7 in this range of Re_{δ_2}. It should be noted here that the turbulence data are not expected to be influenced more than -10% by hot-wire effects which is the maximum reduction of the signal in the range $l^+ < 35$ (see Fernholz and Finley [25], their Fig. 42).

Since the boundary layer becomes rather thin in the acceleration region, measurements of v' and $u'v'$, though made using a miniature cross-wire probe, could not be performed as close to the wall as those of u'. The difficulty of obtaining $u'v'$ close to the wall can, however, be overcome in a FPG boundary layer (see Fernholz and Warnack [21]) because the maximum value of the total shear stress τ_{tot} is at the wall and can thus be determined from measurements of the skin friction. With the interpolated distribution of the total shear stress (see Fernholz and Warnack [21]) and the viscous shear stress calculated from the mean velocity profile, the Reynolds shear stress profile can be extrapolated to the near-wall region. Measured and calculated values of $\overline{u'v'}/u_\tau^2$ are shown in Figs. 11(a) and 11(b). The dashed lines denote the calculated values. The initial profile (Case 1) agrees well with profiles of $\overline{u'v'}/u_\tau^2$ in a canonical boundary layer at the same Re_{δ_2} (e.g. Erm [26]). Its maximum value $-\overline{u'v'}/u_\tau^2$ lies, however, below one due to low Reynolds number effects (see Fernholz and Finley [25], Stefes and Fernholz [19]). Then the Reynolds shear stress profiles decrease sharply since $\bar{\rho}\overline{u'v'}$ lags behind the growth of u_τ until the location of the minimum of Re_{δ_2} and the maximum of H_{12} (approximately) are reached. From here on the Reynolds shear stress increases more strongly than u_τ until a peak value of 0.8 is reached, which is close to values in a ZPG turbulent boundary layer but now with much higher values of $\bar{\rho}\overline{u'v'}$ and u_τ than for the initial profile.

For Case 4 (Fig. 11(b)) the initial profile of $\overline{u'v'}$ shows the greatest effect of the high FST level and this is still visible in the next profile ($x = 1.353$ m) compared with Case 1. The profiles further downstream are dominated again by the FPG and behave similarly to those of Case 1, but the last profile has not yet recovered to ZPG conditions as much as its counterpart in Case 1. A comparison of the Reynolds shear-stress and normal-stress profiles at $x = 1.953$ m shows that the recovery of the shear-stress profiles is, however, more advanced.

The distributions of the Reynolds shear stress and the gradient $\partial\bar{u}/\partial y$ determine the production term of the kinetic energy of the turbulent fluctuations and of $\overline{u'^2}$. The production term $|\overline{u'v'}|\partial\bar{u}/\partial y$ was made dimensionless by u_τ^4 and ν (Rotta [27]) and is plotted against y^+ in Fig. 12. The maximum of the production lies in the buffer layer and reaches a peak value of 0.25 in this scaling. This value is the maximum value for a ZPG boundary layer (Rotta [27]). For Case 4 the profiles are slightly higher compared with Case 1 in the outer region where FPG and FST still interact. As was to be expected, Reynolds normal stress profiles (Figs. 10(a) and 10(b)) and the production profiles show a similar behaviour, except for profile ($x = 1.653$ m) where the

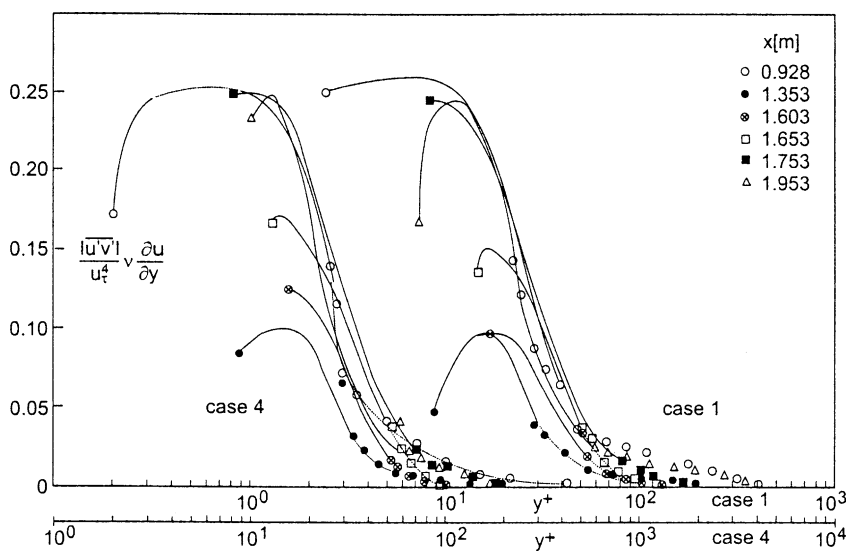

Fig. 12. Distributions of the production term for the turbulent kinetic energy in a turbulent boundary layer with a FPG and FST. Case 1 (low FST), Case 4 (high FST). Symbols denote measured data, lines calculated values.

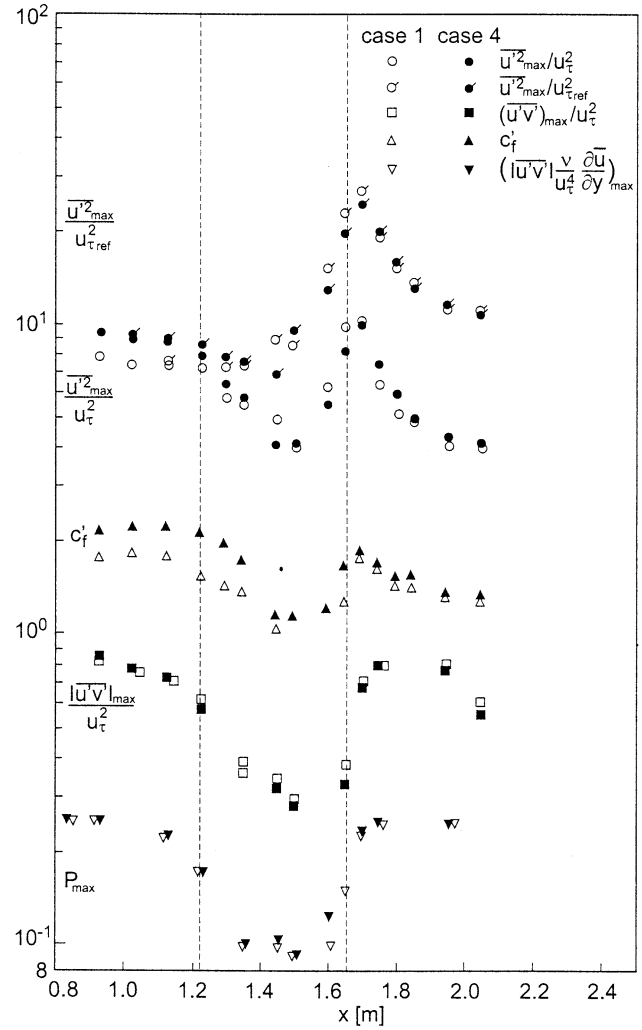

Fig. 13. Streamwise development of the maxima of the Reynolds normal stress and shear stress components, the fluctuating skin friction c_f' and the production term for Cases 1 (low FST) and 4 (high FST).

large values of $\overline{u'^2}$ are not reflected in the production but must be generated by an additional contribution of turbulent transport. Note that the additional production term $\overline{u'^2}\partial\bar{u}/\partial x$ contributes at most 5% of $|\overline{u'v'}|\partial\bar{u}/\partial y$.

Fig. 13 displays an overview of the streamwise development of the maxima of the profiles of the Reynolds normal stress, the Reynolds shear stress and the production as well as the skin-friction fluctuation coefficient $c_f' = 2(\overline{\tau_w'^2})^{1/2}/(\rho_\delta u_\delta^2)$. All streamwise distributions – scaled by $(u_\tau)_{\text{local}}$ – have their first maximum in the upstream region and reach a second maximum at the end of the acceleration region ($x = 1.753$ m). The minimum located between these two maxima coincides approximately with the minimum of Re_{δ_2}. In the ZPG region further downstream, the Reynolds stress peaks decrease, as does c_f', whereas the production maximum remains at its second peak value. Finally, the $(\overline{u'^2})_{\max}$ values, non-dimensionalized by $(u_\tau^2)_{\text{ref}}$ at the reference station ($x = 0.828$ m), are presented in order to show the influence of the FPG and the FST on the absolute value of the Reynolds normal stress. The curve of the peak values shows an increase through the acceleration region by a factor of about 3, independent of the level of the FST, and then decreases from the downstream peak almost to the initial level upstream, indicating that equilibrium is not quite reached. The streamwise development of the curves shown in Fig. 13 agrees again qualitatively with those shown by Fernholz and Warnack [21] and WF [17]. The influence of the FST is confined mainly to the region upstream of the acceleration.

Figs. 14(a) and 14(b) show the profiles of the dimensionless Reynolds normal stress component $\overline{v'^2}/u_\tau^2$ in inner-law scaling for Cases 1 and 4. For Case 1 with low turbulence (Fig. 14(a)) the initial profile shows good qualitative agreement with profiles of

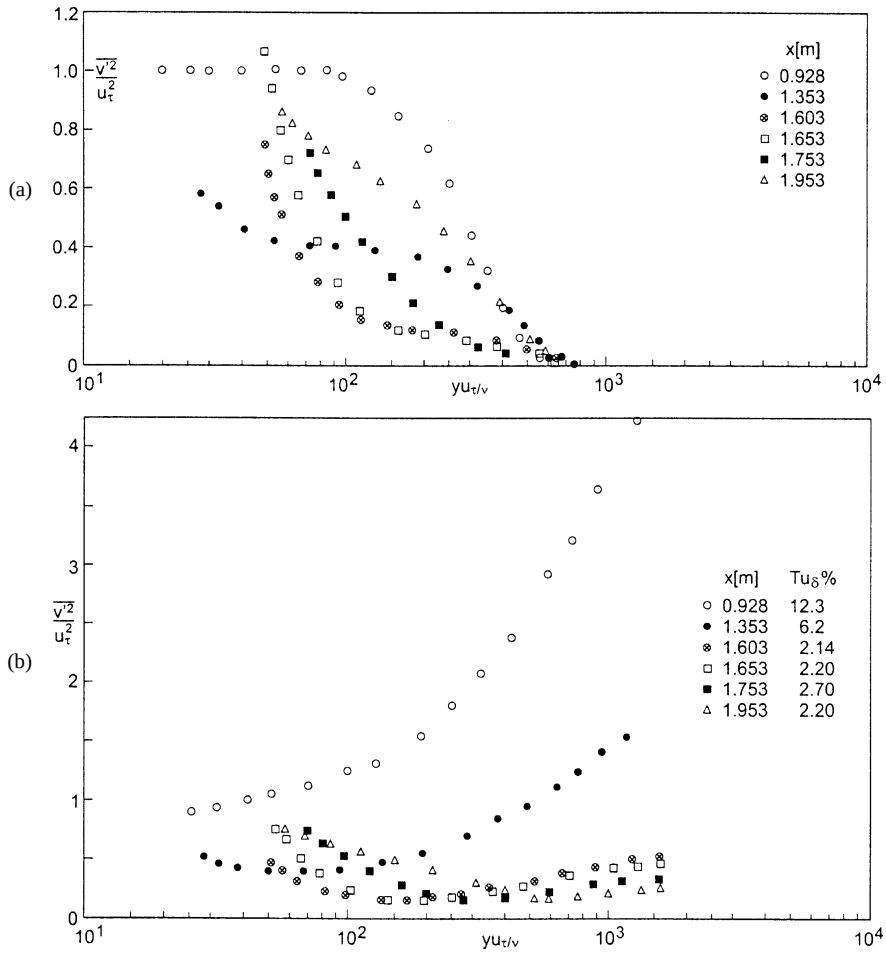

Fig. 14. Profiles of the Reynolds normal stress component $\bar{\rho}\overline{v'^2}$ in inner-law scaling in a turbulent boundary layer with a FPG and FST. (a) Case 1, low FST (symbols as in Fig. 9(a)). (b) Case 4, high FST (symbols as in Fig. 9(b)).

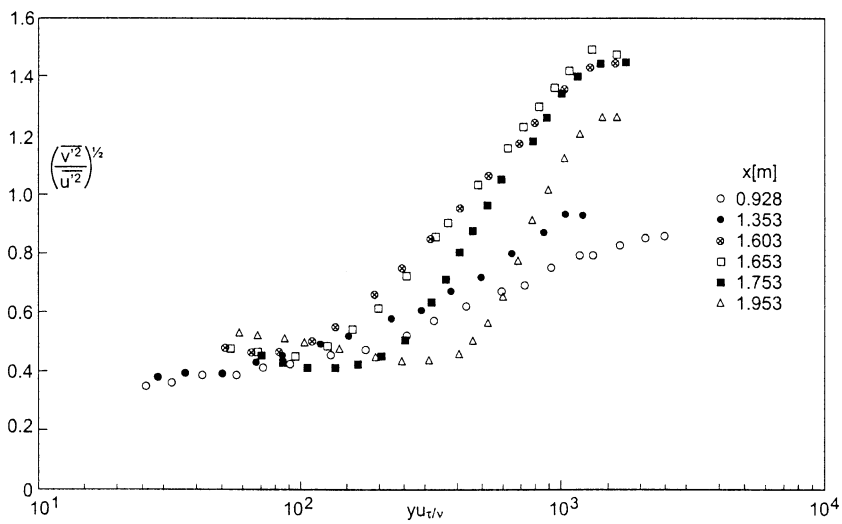

Fig. 15. Distribution of the anisotropy parameter $(\overline{v'^2}/\overline{u'^2})^{1/2}$ in a turbulent boundary layer with a FPG and high FST (Case 4).

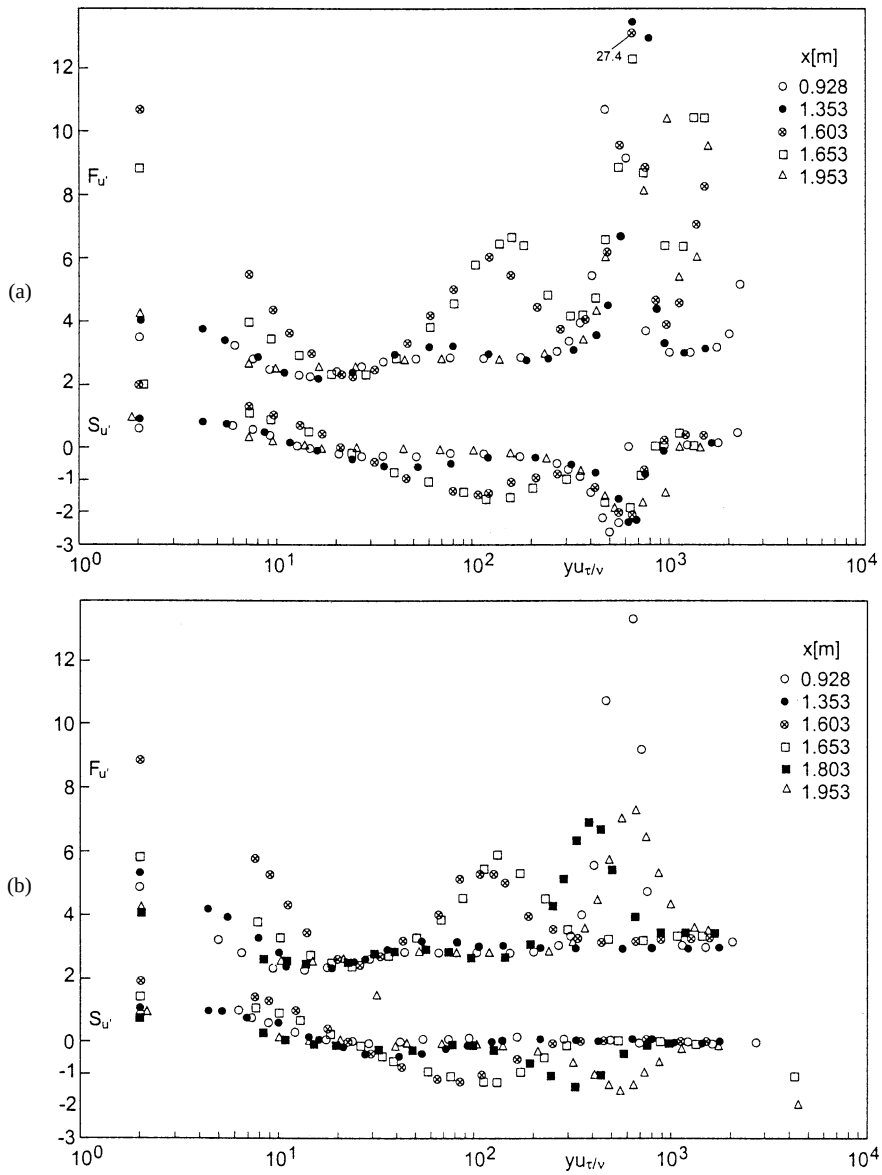

Fig. 16. Profiles of skewness $S_{u'}$ and flatness $F_{u'}$ in a turbulent boundary layer with a FPG and FST. (a) Case 1, low FST. (b) Case 4, high FST.

Erm [26] and Warnack [24] in the same Reynolds number range. In the acceleration region the Reynolds normal stress decreases strongly in the outer region of the boundary layer but rises towards a peak in the log-law region between $1.603 \leqslant x \leqslant 1.653$ m where Warnack [24] found large high-frequency spikes in the time signal of the fluctuating velocity. The last downstream profile ($x = 1.953$ m) shows a recovery to ZPG conditions also in the outer region, but confirms that equilibrium has not been reached. The data measured by Warnack [24] – his Case 2 – are qualitatively well confirmed.

For high FST (Fig. 14(b)) the $\bar{\rho}\overline{v'^2}$-profiles show a similar behaviour in the inner region of the boundary layer where the FPG plays the main role – note the different scale – but behave completely different in the outer region where especially the two upstream profiles rise strongly towards the free-stream with high FST. This rise decreases with decreasing FST in downstream direction.

The anisotropy parameter $(\overline{v'^2}/\overline{u'^2})^{1/2}$ is a structure parameter of the turbulent boundary layer and Fig. 15 presents data for Case 4 (high FST). In the inner region $y^+ \leqslant 150$ the profiles of Case 4 and Case 1 (not shown here, but see WF [17], their Fig. 18, Stefes [20]) are qualitatively similar and independent of the FPG and the FST (see also WF [17], their Fig. 18; Fernholz and Finley [25], their Fig. 62). As we have seen above there are strong effects of both the FPG and the FST in the outer region

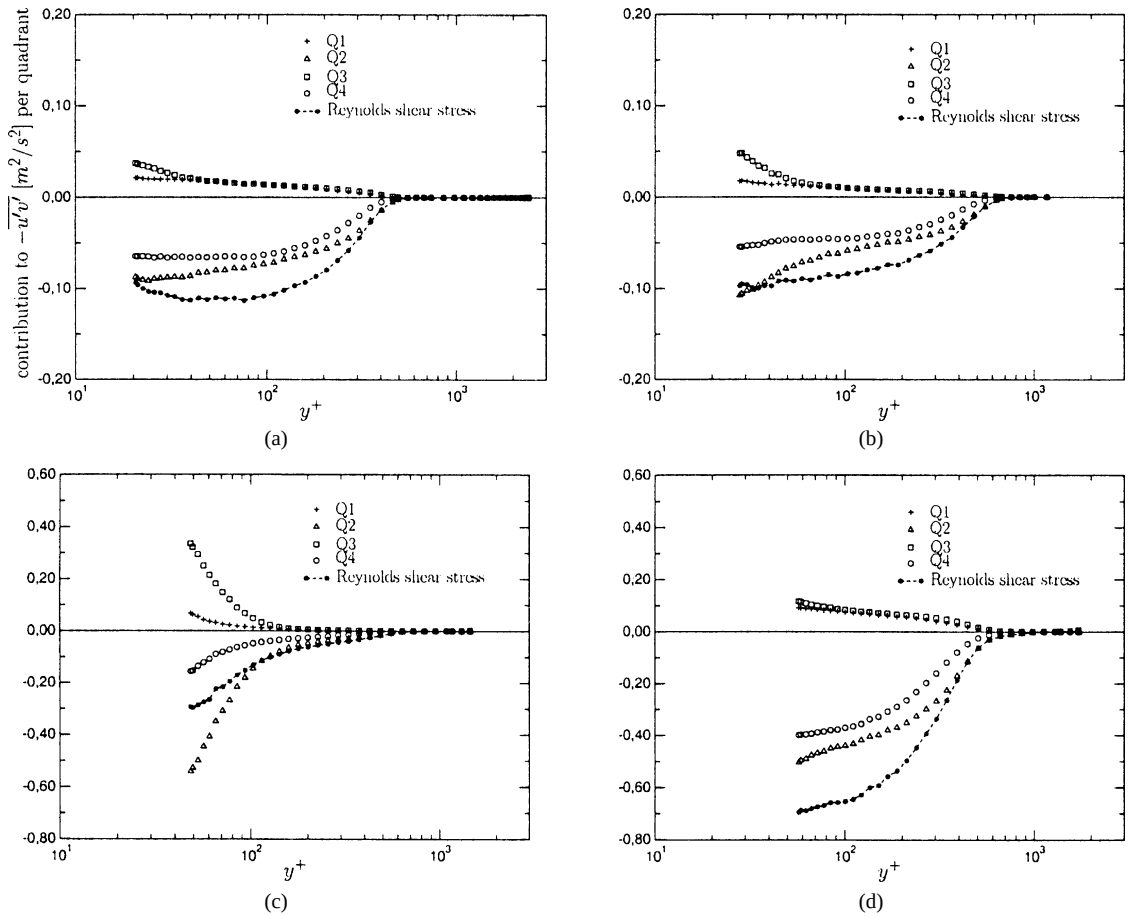

Fig. 17. Profiles of fractional contribution to $-\overline{u'v'}$ per quadrant in a FPG turbulent boundary layer with low FST (Case 1). (a) $x = 0.928$ m, (b) $x = 1.353$ m, (c) $x = 1.653$ m, (d) $x = 1.953$ m.

of the boundary layer. Beyond $y^+ \approx 150$ the anisotropy parameter rises gradually through the acceleration region reaching peak values of about 1.45. This reflects the much stronger decrease of u' towards the edge of the boundary layer. The sharp peak at the outer edge which is characteristic of low FST boundary layers is absent here (see for example Fernholz and Finley [25], their Fig. 62) because the boundary layer edge is less intermittent with FST.

From among the higher moments Figs. 16(a) and 16(b) present the profiles of the skewness $S_{u'}$ and flatness $F_{u'}$ of u' in inner-law scaling for Cases 1 and 4, respectively. The profiles for both cases are qualitatively similar since again the pressure-gradient effect is dominant, but the overall level of the profiles of Case 4 is slightly higher for the two upstream profiles due to the high FST and lower for the profiles in the acceleration region. Here, the turbulence structure is further from relaminarization in Case 4 than in Case 1 and this is reflected in lower values of the flatness (see Warnack [24]). Warnack [24] also noticed first the formation of double troughs of the skewness and double peaks of the flatness in highly accelerated boundary layers. The first peak and the first trough lie in a range $80 \leqslant y^+ \leqslant 200$ and both disappear when the pressure gradient becomes zero again. The second peak of $F_{u'}$ lies in the outer region of the boundary layer showing much larger values for Case 1 since again for Case 4 the edge of the boundary layer is less intermittent due to the FST.

As was observed by Fernholz and Warnack [21] the y^+ position of the maximum of $\overline{u'^2}$, the minimum of $F_{u'}$ and the zero value of $S_{u'}$ coincide within a narrow range of y^+. This range is $14 \leqslant y^+ \leqslant 25$, slightly higher than for a ZPG boundary layer ($y^+ \approx 14$), and practically unaffected by the FST level.

The development of the Reynolds shear-stress profiles under the influence of FST and FPG can be studied in more detail if a quadrant decomposition of the fluctuating streamwise and normal velocity components is made (e.g. Wallace et al. [28]). The profiles are not made dimensionless here, in order to show the change of the absolute value of $-\overline{u'v'}$ at the four streamwise x-positions and thus to complement Figs. 11(a) and 11(b). The four fractional contributions to $-\overline{u'v'}$ are shown in Figs. 17

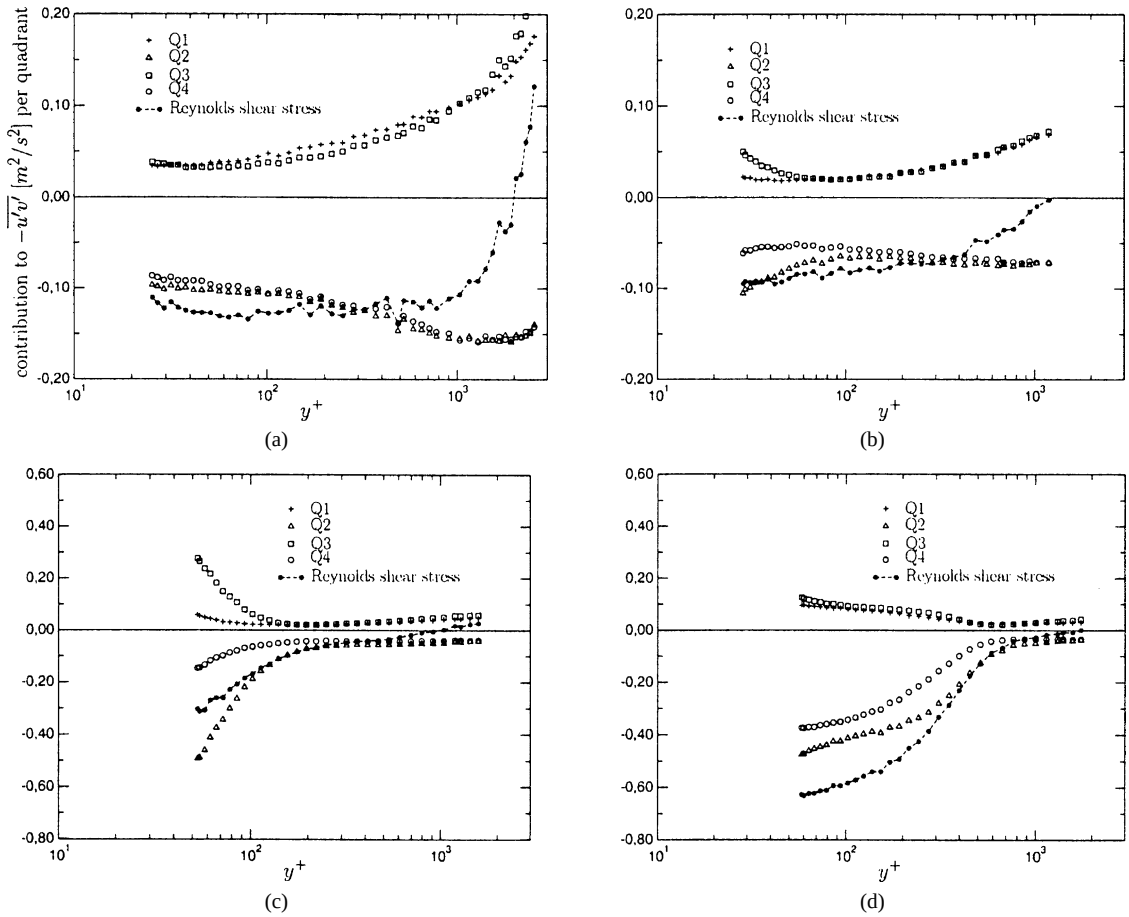

Fig. 18. Profiles of fractional contribution to $-\overline{u'v'}$ per quadrant in a FPG turbulent boundary layer with high FST (Case 4). (a) $x = 0.928$ m, (b) $x = 1.353$ m, (c) $x = 1.653$ m, (d) $x = 1.953$ m.

(Case 1) and 18 (Case 4). The events in quadrants Q2 and Q4 can be associated with ejections ($u' < 0, v' > 0$) and sweeps ($u' > 0, v' < 0$) and those in Q1 and Q3 with outward ($u' > 0, v' > 0$) and inward ($u' < 0, v' < 0$) interactions. At all streamwise stations the events of quadrants 2 and 4 contribute most to $-\overline{u'v'}$ as had been observed previously by Wallace et al. [28] and Willmarth and Lu [29], for example, who investigated fully turbulent channel flow and a ZPG turbulent boundary layer. This trend is confirmed when FST and FPG effects occur. The quadrant contributions are affected mainly by FST in the outer region and by the FPG in the inner region of the boundary layer. Independent of FST and FPG the Q2 contributions are largest in the y^+ range investigated here confirming the results of Wallace et al. [28]. Fig. 17 presents the contributions of the four quadrants and $-\overline{u'v'}$ against y^+ and shows the influence of the FPG which reduces all contributions in the outer region (Figs. 17(b) and 17(c)) compared with Fig. 17(a) where the pressure gradient is zero. Fig. 17(c) shows a large increase of the Q2 but also of the Q3 contribution and in the relaxation region a further increase of Q2 and Q4 as well as a reduction of Q3 (Fig. 17(d)). A comparison of Figs. 17(d) and 18(d) shows a similar behaviour of the relaxing boundary layer in Cases 1 and 4 with only a small influence of FST on the outer region in Fig. 18(d), but no similarity with the profiles of the initial ZPG boundary layer (Figs. 17(a) and 18(a)). Fig. 18(a) displays the contributions of the four quadrants under the influence of high FST in a ZPG boundary layer where the influence of the FST on the contributions Q1 to Q4 is very strong in the outer region with even a change in sign of $-\overline{u'v'}$ due to the high contributions of Q1 and Q3. The profiles in Fig. 18(b) show a strong interactive effect of both FST and FPG whereas in Fig. 18(c) the pressure gradient effect is dominant, almost as in Fig. 17(c), reducing the contributions of all quadrants in the outer region and increasing the contributions of Q2 to Q4 in the inner region.

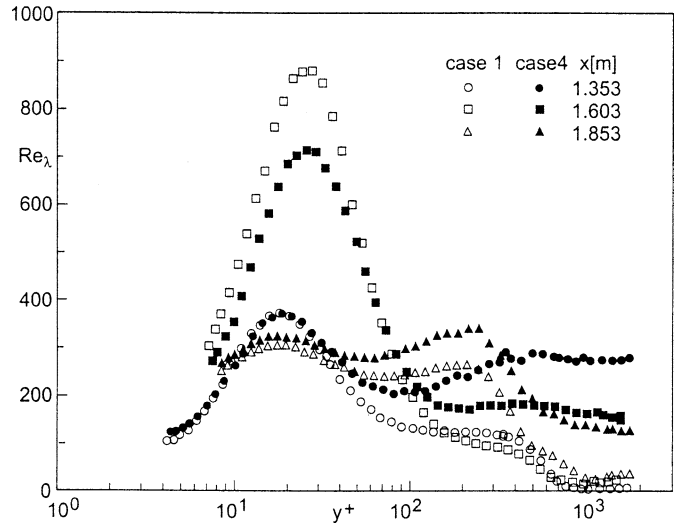

Fig. 19. Profiles of the turbulent Reynolds number of three streamwise stations for Cases 1 (low FST) and 4 (high FST).

6. Spectra

The influence of high FST on the spectra of the velocity component u' in a ZPG boundary layer was investigated by Thole and Bogard [14] and Stefes and Fernholz [19], for example. The data acquired by the latter authors were taken in the same test section as those of the present investigation, but with the centre body removed and are therefore not repeated here. The spectra included here were influenced both by strong FPG and by FST. Three characteristic stations were selected. The first station ($x = 1.353$ m) is just upstream of the peak of the acceleration parameter K. The second station ($x = 1.603$ m) is where Re_{δ_2} and c_f are close to their respective minima and H_{12} and the turbulent Reynolds number Re_λ at their respective maxima. The third is where the pressure gradient has abated, but the upstream history effect is still present ($x = 1.853$ m). The turbulent Reynolds number $Re_\lambda = \lambda u'_{\rm rms}/\nu$ is an important parameter besides the pressure gradient parameter and the turbulence level. The Taylor microscale λ was calculated from the dissipation rate D_{11} of the one-dimensional spectrum

$$D_{11} = 2\nu \int_0^\infty k_1^2 E_{u1}(k_1)\,\mathrm{d}k_1 = 2\nu \overline{\left(\frac{\partial u'}{\partial x}\right)^2} = 2\nu \frac{\overline{u'^2}}{\lambda^2}. \tag{4}$$

The profiles at the above three stations for Cases 1 and 4 are presented in Fig. 19. The profiles with high FST have a double peak, one in the vicinity of the wall ($16 \leqslant y^+ \leqslant 25$) and the other in the outer layer ($85 \leqslant y^+ \leqslant 550$). The location of the first peak is practically independent of the FST and moves towards the higher values of y^+ with the rise of the FPG. For Case 1 the second peak disappears when the boundary layer is accelerated showing the strong effect of the FPG on the turbulence structure in the outer region.

Figs. 20 and 21 present examples of the spectra, first at the location of $(Re_\lambda)_{\max}$, i.e. in the near-wall region ($16 \leqslant y^+ \leqslant 25$), at three selected streamwise stations and then at $x = 1.603$ m at three wall-normal distances ($y^+ = 25$, 100 and at $y/\delta_{99.5} = 1$) for Cases 1 and 4.

The longitudinal wavenumber spectrum $E_{11}(k_1)$ – where $k_1 = 2\pi f/\bar{u}$ is the wavenumber, f the frequency and $\bar{u}$ the mean velocity – is usually scaled by $v_k^2\eta = (\epsilon\nu^5)^{1/2}$ and plotted against $k_1\eta = k_1(\nu^3/\epsilon)^{1/4}$. Here η denotes the Kolmogorov microscale, v_k the Kolmogorov velocity and ϵ the dissipation of the turbulence energy.

For ZPG and low FST the dimensionsless longitudinal wavenumber spectrum is

$$E_{11}/(v_{k_1}^2\eta) = F(k_1\eta, Re_\lambda). \tag{5}$$

In this scaling two spectra are equal if Re_λ is the same. In flows with FST and pressure gradients it must be expected that E_{11} depends also on Tu_δ and K.

Fig. 20 shows spectra in the near-wall region ($y^+ \approx 20$) where Re_λ has its maximum at the three streamwise stations. The pressure gradient is the same at each station in Cases 1 and 4 but Re_{δ_2} and Tu_δ are different. At $x = 1.353$ m the turbulent Reynolds numbers are equal and so are the spectra. At the other two locations x the spectra have values of Re_λ which are slightly different and they follow the Re_λ trend, i.e. the spectrum with the higher Reynolds number lies above that with the

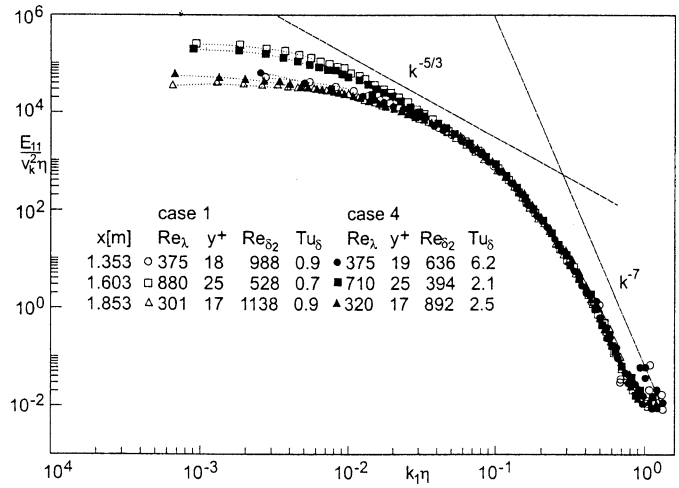

Fig. 20. One-dimensional spectra in Kolmogorov scaling at three streamwise stations at the location y^+ where Re_λ has its maximum for Cases 1 (low FST) and 4 (high FST).

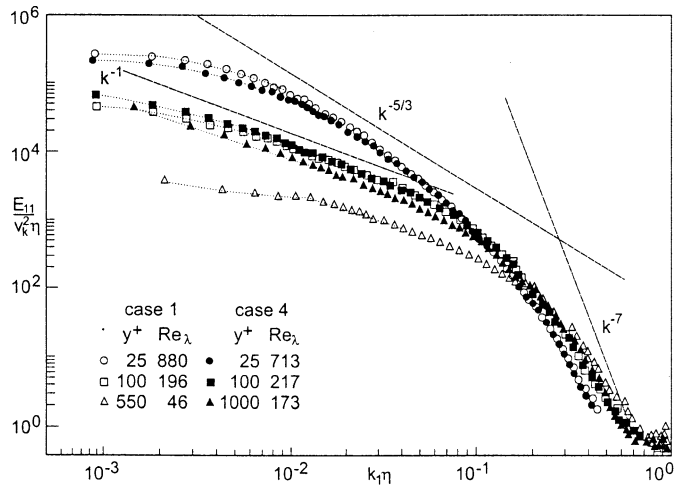

Fig. 21. One-dimensional spectra in Kolmogorov scaling at three wall-normal locations at $x = 1.603$ m for Cases 1 (low FST) and 4 (high FST).

lower Re_λ, irrespective of the FST. There is, however, an influence of the FST in the lower wavenumber range (e.g. Stefes and Fernholz [19]).

Fig. 21 presents spectra at three locations normal to the wall at $x = 1.603$ m for the two cases. The spectra follow the trend seen already in Fig. 20, whereby spectra for higher turbulent Reynolds number Re_λ exhibit higher levels at lower wavenumbers. At these relatively low levels of the FST the turbulent Reynolds number appears to be the dominating parameter.

Figs. 20 and 21 contain dashed lines which characterize the inertial subrange of the equilibrium spectrum ($E \sim k^{-5/3}$), at higher wavenumbers ($E \sim k^{-7}$) and in the lower wavenumber range ($E \sim k^{-1}$). Fig. 20, which presents spectra for values of y^+ which correspond to maximum values of Re_λ, shows that the agreement with the $k^{-5/3}$ line extends over a larger wavenumber range for the spectra with the higher Re_λ. The influence of the FST is negligible in the inner region of the boundary layer at these relatively low levels. With decreasing Re_λ at a fixed streamwise location (Fig. 21), the spectra depart earlier from the $k^{-5/3}$ behaviour and follow the k^{-1} trend in the lower wavenumber range as has been noticed by Warnack [24] and Stefes and Fernholz [19].

7. Discussion

The aim of this experimental study has been to investigate the influence of high FST and a strong favourable pressure gradient on a turbulent boundary layer, especially on the relaminarization region which was found to exist (WF [17]) when the FST level was very low ($Tu_\delta \leqslant 0.1\%$). Since FST increases the skin friction, it was expected that the dominating effect of the FPG could be counteracted so that relaminarization would not occur. This is true only for very high levels of FST, generated by jets injected normal to the free stream upstream of the test boundary layer (Thole et al. [12]). The high FST affects the properties of the boundary layer mainly in two ways. Firstly, the mean velocity profiles in the initial region are fuller and their skin friction is 30% higher than with low FST. Secondly, initially higher values of FST and skin friction both remain higher in the streamwise direction.

The FST in the streamwise direction decays strongly due to the favourable pressure gradient, whereas the ratio of the integral length scale Λ_{11} and the boundary layer thickness $\delta_{99.5}$ increase from O(1) to O(10) through the acceleration region. These two effects reduce the effectiveness of the FST on the boundary layer. According to the results discussed by Hancock and Bradshaw [10] in ZPG boundary layers the ratio $\Lambda_{11}/\delta_{99.5}$ should be of O(1) to have the greatest effect of the FST on the mean flow. In Case 4 the ratio $\Lambda_{11}/\delta_{99.5}$ is influenced mainly by the large fall in $\delta_{99.5}$ whereas in Case 1 the decrease of $\delta_{99.5}$ is less and the rise of Λ_{11} larger. FST not only increases the mean skin friction, but also decreases the shape parameter H_{12}. Wall shear stress fluctuations increase with FST and so do skewness $S_{\tau_w'}$ and flatness $F_{\tau_w'}$.

As for the mean velocity profiles the FST counteracts the FPG effect on the mean velocity profiles, by rendering the departure from the standard logarithmic law smaller and thus slows down the development towards a laminar-like profile (see WF [17]). The main effect occurs, however, in the wake region. As for the turbulence quantities, the maximum values of the Reynolds stresses, nondimensionalized by the skin-friction velocity u_τ, and c_f' show only a small effect in the upstream ZPG region where FST is high, but are largely dominated by the favourable pressure gradient downstream. FST has a large effect on the profiles of the Reynolds stresses in the outer region, strongest on the Reynolds normal stress component $\overline{v'^2}/u_\tau^2$ and the anisotropy parameter $v'_{\mathrm{rms}}/u'_{\mathrm{rms}}$. The profiles of the turbulent Reynolds number Re_λ are affected both by the FST and the FPG but for the spectra in Kolmogorov scaling Re_λ is the dominating parameter.

Acknowledgement

We acknowledge the reviewing of Dr. Roger Kinns and the financial support of the first author by DFG.

References

[1] B.J. Abu-Ghannam, R. Shaw, Natural transition of boundary layers. The effect of turbulence, pressure gradient and flow history, J. Mech. Eng. Sci. 22 (1980) 213–228.
[2] P.E. Roach, D.H. Brierly, The influence of a turbulent freestream on zero pressure gradient transitional boundary layer development including the condition test cases T3A and T3B, in: O. Pironneau, et al. (Eds.), Numerical Simulation of Unsteady Flows and Transition to Turbulence, Cambridge University Press, Cambridge, 1989.
[3] R.E. Mayle, The role of laminar-turbulent transition in gas turbine engines, ASME J. Turbomachinery 113 (1991) 509–535.
[4] M.F. Blair, Boundary-layer transition in accelerating flows with intense freestream turbulence: part 1 – disturbances upstream of transition onset, ASME J. Fluids Eng. 114 (1992) 313–321.
[5] M.F. Blair, Boundary-layer transition in accelerating flows with intense freestream turbulence: part 2 – the zone of intermittent turbulence, ASME J. Fluids Eng. 114 (1992) 322–332.
[6] R.E. Mayle, K. Dullenkopf, A. Schulz, The path to predicting bypass transition, ASME J. Turbomachinery 119 (1997) 405–411.
[7] M. Blair, Influence of free-stream turbulence on turbulent boundary layer heat transfer and mean profile, part I – experimental data, ASME J. Heat Transfer 105 (1983) 33–40.
[8] M. Blair, Influence of free-stream turbulence on turbulent boundary layer heat transfer and mean profile, part II – analysis of results, ASME J. Heat Transfer 105 (1983) 41–47.
[9] I.P. Castro, Effects of free-stream turbulence on low Reynolds number boundary layers, Trans. ASME J. Fluids Eng. 106 (1984) 298–306.
[10] P. Hancock, P. Bradshaw, The effect of free-stream turbulence on turbulent boundary layers, ASME J. Fluids Eng. 105 (1983) 284–289.
[11] P. Hancock, P. Bradshaw, Turbulence structure of a boundary layer beneath a turbulent free stream, J. Fluid Mech. 205 (1989) 45–76.
[12] K. Thole, D. Bogard, J. Whan, Generating high freestream turbulence levels, Exp. Fluids 17 (1994) 375–380.
[13] K. Thole, D. Bogard, Enhanced heat transfer and shear stress due to high free-stream turbulence, ASME J. Turbomachinery 117 (1995) 418–424.
[14] K. Thole, D. Bogard, High freestream turbulence effects on turbulent boundary layers, ASME J. Fluids Eng. 118 (1996) 276–284.
[15] K. Rued, S. Wittig, Laminar and transitional boundary layer structures in accelerating flow with heat transfer, ASME J. Turbomachinery 108 (1986) 116–123.

[16] R.J. Volino, T.W. Simon, Boundary layer transition under high free-stream turbulence and strong accelerated conditions: part 1 – mean flow results, part 2 – turbulent transport results, ASME J. Heat Transfer 119 (1997) 420–432.
[17] D. Warnack, H.-H. Fernholz, The effects of a favourable pressure gradient and of the Reynolds number on an incompressible axisymmetric turbulent boundary layer. Pt. 2. The boundary layer with relaminarization, J. Fluid Mech. 359 (1998) 357–381.
[18] R. Narasimha, The three archetypes of relaminarization, in: Proc. 6th Canadian Congr. Appl. Mech., Vancouver, 1977.
[19] B. Stefes, H.-H. Fernholz, Skin friction and turbulence measurements in a boundary layer with zero-pressure-gradient under the influence of high intensity free-stream turbulence, Eur. J. Mech. B Fluids 23 (2004) 303–318.
[20] B. Stefes, Turbulente Wandgrenzschichten mit und ohne negativen Druckgradienten unter dem Einfluss hoher Turbulenzintensitäten in der Aussenströmung, Dissertation, Technische Universität Berlin, 2003.
[21] H.-H. Fernholz, D. Warnack, The effects of a favourable pressure gradient and of the Reynolds number on an incompressible axisymmetric turbulent boundary layer. Pt. 1. The turbulent boundary layer, J. Fluid Mech. 359 (1998) 329–356.
[22] B.E. Launder, Laminarization of the turbulent boundary layer by acceleration, MIT Gas Turbine Lab. Rep. 77, 1964.
[23] V.C. Patel, Calibration of the Preston tube and limitations on its use in pressure gradients, J. Fluid Mech. 23 (1965) 185–208.
[24] D. Warnack, Eine experimentelle Untersuchung von beschleunigten turbulenten Wandgrenzschichten, Dissertation, Technische Universität Berlin, 1996.
[25] H.-H. Fernholz, P.J. Finley, The incompressible zero-pressure-gradient turbulent boundary layer: an assessment of the data, Prog. Aerospace Sci. 32 (1996) 245–311.
[26] L.P. Erm, Low Reynolds-number turbulent boundary layer, Ph.D. thesis, University of Melbourne, 1988.
[27] J.C. Rotta, Turbulent boundary layers in incompressible flow, in: Progr. Aeronaut. Sci., vol. 2, Pergamon Press, Oxford, 1962, pp. 1–221.
[28] J.M. Wallace, H. Eckelmann, R.S. Brodkey, The wall region in turbulent shear flow, J. Fluid Mech. 54 (1972) 39–48.
[29] W.W. Willmarth, S.S. Lu, Structure of the Reynolds stress near the wall, J. Fluid Mech. 55 (1972) 65–92.